INTERNATIONAL JOURNAL OF INTEGRATED ENGINEERING
ISSN: 2229-838X e-ISSN: 2600-7916

IJIE

Vol. 17 No. 1 (2025) 451-462
https://publisher.uthm.edu.my/ojs/index.php/ijie

Development of Optical Sensor Using ZnO Microflowers as Sensing Material for Organophosphate Pesticide Detection

Natasya Salsabiila[1,2,3], Suratun Nafisah[1]*, Bambang Irawan Tanjung[1], Nur Liyana Razali[2,3], Marlia Morsin[2,3], Lukman Nulhakim[4], Muhammad Reza Kahar Aziz[1]

[1] *Department of Electrical Engineering, Institut Teknologi Sumatera, 35365 Jatiagung, Lampung Selatan, INDONESIA*
[2] *Faculty of Electrical and Electronic Engineering, Universiti Tun Hussein Onn Malaysia, 86400 Parit Raja, Batu Pahat, Johor, MALAYSIA*
[3] *Microelectronics and Nanotechnology – Shamsuddin Research Centre (MiNT-SRC), Institute of Integrated Engineering, Universiti Tun Hussein Onn Malaysia, 86400 Parit Raja, Batu Pahat, Johor, MALAYSIA*
[4] *Technology Development I, PT. Pertamina (Holding), 12710, South Jakarta, INDONESIA*

*Corresponding Author: suratun.nafisah@el.itera.ac.id
DOI: https://doi.org/10.30880/ijie.2025.17.01.036

Article Info

Received: 26 September 2024
Accepted: 29 November 2024
Available online: 30 April 2025

Keywords

Diazinon, optical sensor, organophosphate pesticide, profenofos, ZnO

Abstract

A widely utilized organophosphate pesticide for crop pest control, profenofos and diazinon, have been categorized as moderately toxic by the World Health Organization (WHO). Hence, the identification of profenofos and diazinon residues holds importance for ensuring food safety. This study focuses on the alternative profenofos and diazinon detection method utilizing optical sensors, offering a label-free and real-time measurement scheme. The sensor utilizes zinc oxide (ZnO) with a microflowers structure (ZnO MFs) as the sensing material, chosen for its enlarged surface area, which enhances sensitivity to alterations in the surrounding medium. Synthesized via the solution route method, the ZnO MFs exhibit dimensions of 5.47 ± 0.84 µm in length, 1.30 ± 0.26 µm in width, and an aspect ratio of 4.35 ± 1.02. Profenofos and diazinon concentrations ranging from 1 to 10,000 ppm are used as targeted analytes for sensor testing. The findings demonstrate distinct responses of the optical sensor, with a detection limit (LoD) of 1 ppm. The sensing parameter, Absolute Optical Change (AOC), exhibits its highest value at 1 ppm for profenofos and 100 ppm for diazinon, indicating an optimal sensitivity. In conclusion, optical sensors using ZnO MFs as sensing material offer a good potential to be used as an alternative method for pesticide detection, with further improvement in LoD and sensitivity aspects needed.

1. Introduction

Organophosphate pesticides, comprised of chemical compounds derived from phosphoric acid, are extensively utilized as herbicides, insecticides, and fungicides due to their efficacy in pest control. These compounds exert

their pesticidal activity by targeting acetylcholinesterase (AChE), an enzyme responsible for catalyzing the breakdown of the neurotransmitter acetylcholine [1]. The inhibition of AChE by organophosphates disrupts the normal functioning of the nervous system in pests, leading to hyperstimulation of nerve cells, paralysis, and eventual mortality [2]. However, the broad-spectrum toxicity of organophosphates extends beyond pests, posing significant risks to human health by inhibiting AChE in non-target organisms [3]. Exposure to organophosphate pesticides can occur through various routes, including inhalation, ingestion of contaminated food or water, and dermal contact [4]. Chronic exposure to even low levels of organophosphates has been associated with a spectrum of adverse health effects, including neurological disorders, developmental abnormalities in children, and an elevated susceptibility to certain cancers [5].

Organophosphate pesticides that are widely used are profenofos and diazinon, which reach 70 % of use to combat pests infesting crops [6], [7]. Its mechanism of action involves the inhibition of acetylcholinesterase (AChE), leading to respiratory distress, prompting the World Health Organization (WHO) to designate profenofos and diazinon as a moderately toxic pesticide (category II pesticide). Additionally, regulatory bodies such as the Food and Agriculture Organization and the Codex Committee have established a permissible range for daily non-toxic intake, typically falling between 0 and 0.03 mg/kg body weight [8]. Notably, residues of profenofos and diazinon can persist on crops post-application, with the potential to endure through harvesting and subsequent processing stages [9]. Therefore, the imperative of detecting profenofos and diazinon is underscored not only to safeguard food safety but also to ensure compliance with stringent regulatory standards governing pesticide residues in agricultural produce.

Various techniques are employed for the detection of profenofos, encompassing gas chromatography, enzyme-linked immunosorbent assay (ELISA), and mass spectrometry methodologies. Gas chromatography involves the vaporization of the sample, which then traverses a chromatographic column for component separation. Quantification of profenofos within the sample is achieved using detectors such as flame ionization detector (FID) or electron capture detector (ECD) [10]. For example, Ashraf *et al.* demonstrated the efficacy of this method, achieving a limit of detection (LoD) of 0.05 mg/kg [11]. Conversely, ELISA employs incubation of the sample with an enzyme-labeled antibody, followed by measurement of enzyme activity to ascertain analyte concentration. While ELISA offers rapid sensitivity, it necessitates specific antibodies for profenofos detection [12]. For instance, Kuo-Hui *et al.* utilized this technique, employing 20 nm Ag nanoparticles as the sensing material immobilized by polyclonal antibodies [13]. Alternatively, mass spectrometry entails ionization of the sample for mass-to-charge ratio analysis of ions [14]. Dusit *et al.* reported coupling mass spectrometry with electrospray ionization for profenofos detection [15].

In the realm of diazinon detection, various methodologies have been explored, including electrochemical analysis, visible/near-infrared (VIS/NIR) spectroscopy, and High-Performance Liquid Chromatography (HPLC). Electrochemical approaches involving the utilization of electrochemical sensors and biosensors have garnered attention for diazinon detection. For instance, Fatemeh *et al.* employed an electrochemical approach and achieved a remarkable detection limit of 4.5×10^{-10} M, with a tested concentration range of 1×10^{-10} to 6×10^{-8} M [16]. VIS/NIR spectroscopy has also emerged as a non-destructive means for diazinon residue detection. Bahareh *et al*. illustrated the efficacy of this method in cucumber plants, achieving a standardized error of cross-validation value of 0.366 [17]. Furthermore, HPLC methodology offers a comprehensive approach involving the extraction of diazinon from samples, chromatographic separation, absorbance-based detection, and quantification through calibration curves. Reza *et al.* enhanced this method by incorporating Nebulizer-Assisted Liquid-Phase Microextraction (NALPME), resulting in detection and quantification limits of 0.123 µg/mL and 0.372 µg/mL, respectively [18].

In this study, an innovative profenofos and diazinon detection approach based on optical sensors is proposed. Leveraging the optical phenomenon exhibited by micromaterials under specific wavelengths of light, optical sensors offer a label-free detection mechanism, circumventing the need for complex labeling procedures that risk sample contamination [19]. Additionally, optical sensors afford real-time monitoring of analyte binding events, facilitating dynamic measurement capabilities [20].

In this investigation, zinc oxide (ZnO) emerges as the chosen sensing material for the optical sensor. ZnO is favored for its remarkable sensitivity to environmental changes, particularly its responsiveness to the presence of profenofos and diazinon [6], [21]. Moreover, ZnO offers the advantageous attributes of being environmentally benign and non-toxic, essential considerations for applications in environmental monitoring and food safety [22]. The selection of the microflower structure for ZnO is deliberate, driven by its larger surface area, enhancing its sensitivity to the target analyte [23].

Prior research has explored the utility of ZnO microflowers (ZnO MFs) as sensing materials for detecting various hazardous substances with potential human health implications. For instance, Yingnan *et al.* employed ZnO MFs to detect water pollutant bisphenol A with a detection limit of 1 nM [24]. Similarly, Ahmad *et al.* utilized ZnO MFs for formaldehyde detection with response and recovery times of 65 s and 117 s, respectively [25]. Additionally, Wenzhi *et al.* employed ZnO MFs for H_2S detection with a response time of 157.3 s [26]. While ZnO

Int. Journal of Integrated Engineering Vol. 17 No. 1 (2025) p. 451-462

has predominantly been utilized for sensing gaseous analytes, this study presents an innovative application by employing ZnO MFs for the detection of profenofos and diazinon in solution form.

2. Experimental

2.1 Synthesis of ZnO Microflowers

This study involves the synthesis of ZnO MFs utilizing the solution route method, adapted from a previous study [27]. Specifically, a solution comprising 0.3 M of zinc acetate dihydrate ($Zn(CH_3COO)_2.2H_2O$) diluted in 100 mL of deionized water is prepared, with the addition of 3 M sodium hydroxide (NaOH). Subsequently, the resulting white-colored solution undergoes stirring at 300 rpm for 10 minutes while maintaining a temperature of 60°C. This prepared solution is then subjected to characterization utilizing Ultra Violet-Visible (UV-Vis), X-Ray Diffraction (XRD), and Field Emission Scanning Microscopy (FESEM) to obtain the optical, structural, and morphological properties of ZnO MFs.

UV-Vis analysis is conducted employing the UV-1800 Shimadzu UV-Vis Spectrophotometer, Japan, operating within a defined wavelength range of 300 to 500 nm. The 3 mL of ZnO solution is placed in a cuvette for the measurement. Subsequently, XRD characterization is performed utilizing the Bruker D8 Advance X-Ray Diffractometer, Germany, with CuKα radiation (λ = 1.5406 Å) and a diffraction angle range spanning 20^0 to 60^0. FESEM investigations are carried out using the Joel JSM-7600 Field Emission Scanning Electron Microscope, USA, operating at an accelerating voltage of 5 kV, with a magnification of 1,000X. For XRD and FESEM characterization, the ZnO MFs solution must be left undisturbed for 1 hour. After 1 hour, the supernatant is removed and rinsed using deionized water. Then, the residue is dried in an oven at 100^0 C until ZnO powder forms.

2.2 Analyte Preparation

The commercialized profenofos 500 EC (brand Curacron, Indonesia) and diazinon 600 EC (supplied by Petrokimia Kayaku, Indonesia) are selected as the targeted analytes for this study due to their advantageous characteristics, particularly their flexibility in controlling concentration levels. By utilizing commercial profenofos and diazinon, the experimentation process benefits from consistent and controlled conditions, ensuring reliable and reproducible results. The profenofos and diazinon samples, ranging from 1 to 10,000 ppm, are meticulously prepared by diluting the commercial stock with deionized water (DIW) using the formula:

$$M_1V_1 = M_2V_2 \quad (1)$$

where M_1 is the initial concentration, V_1 is the initial volume, M_2 is the final concentration, and V_2 is the final volume.

2.3 Optical Sensor System Setup

The optical sensor setup employed in this investigation draws adaptation from a precedent study focused on herbicide and glucose detection via absorbance mode [28]–[30]. Specifically, for profenofos and diazinon detection, the optical sensor configuration encompasses essential components such as a light source, fiber optic, chamber, spectrometer, and a computer equipped with analytical software. The selected light source is the AvaLight-HAL-(S)-Mini halogen lamp, chosen for its compatibility with the intended application. Fiber optic cables of simplex design, namely FC-UVIR200-1/FC-UVIR400-1, are utilized to facilitate efficient light transmission. Previous research endeavors involving duplex fiber optics have addressed diverse analytes, including glyphosate, boric acid, and formaldehyde detection via reflectance mode [31]–[33]. The self-made chamber boasts a cube-shaped design featuring strategically positioned apertures on the right and left sides to accommodate sensor components. Notably, the chamber dimensions measure 3 cm x 3 cm x 3.56 cm, ensuring optimal compatibility with the experimental setup. The spectrometer utilized is the AvaSpec-Mini2048CL, complemented by AvaSoft software for data analysis and interpretation. The light source, simplex fiber optic, spectrometer, and software analyzer are purchased from Avantes. The sensor setup is elucidated in Figure 1, while Figure 2 provides detailed dimensions of the custom-made chamber.

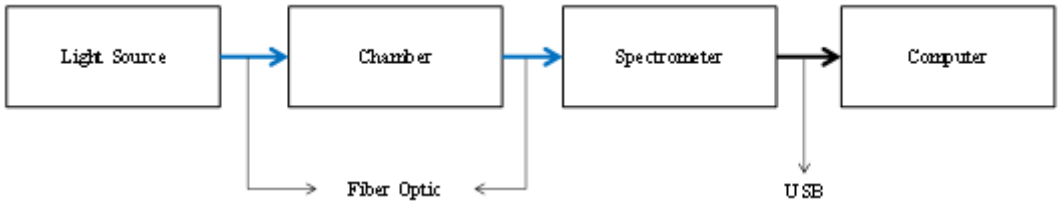

(a)

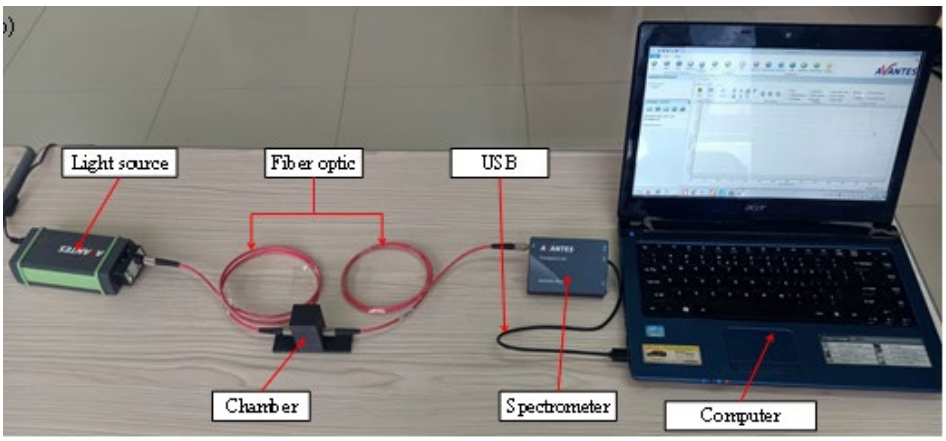

(b)

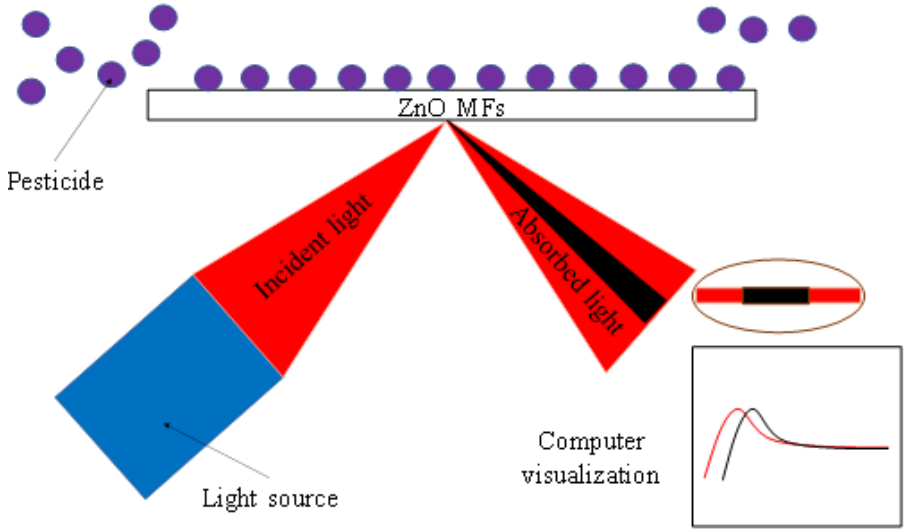

(c)

Fig. 1 *Optical sensor (a) Block diagram; (b) Setup system; and (c) Working principle*

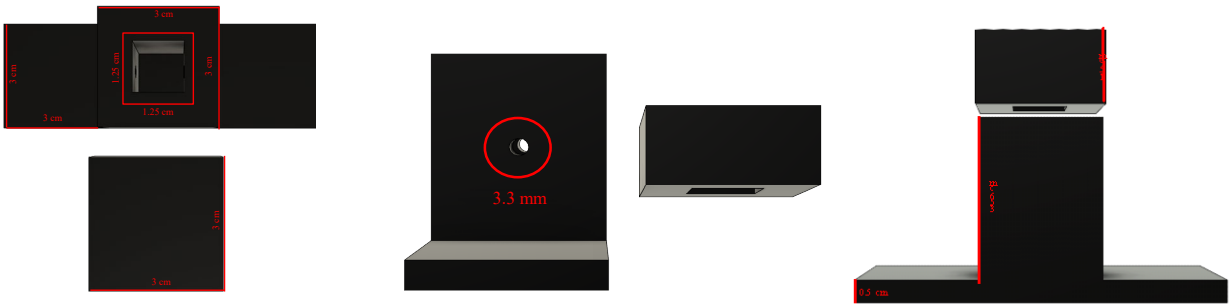

(a) (b) (c)

Fig. 2 *Chamber size and dimension from (a) Top; (b) Side; and (c) Front view*

Int. Journal of Integrated Engineering Vol. 17 No. 1 (2025) p. 451-462

3. Results and Discussion

3.1 Characterization of ZnO Microflowers as Sensing Material

Figure 3 depicts the ZnO MFs synthesized via a simple route method, both in solution and powder forms, facilitating further characterization. These ZnO MFs exhibit a well-defined nanorod structure. The synthesis process of ZnO MFs in solution form is outlined as follows.

$$Zn(CH_3COO)_2.2H_2O + 2NaOH \rightarrow Zn(OH)_2 + 2CH_3COONa + 2H_2O \quad (2)$$

$$Zn(OH)_2 + 2H_2O \rightarrow [Zn(OH)_4^{2-}]^{2+} + 2H^+ \quad (3)$$

$$[Zn(OH)_4^{2-}]^{2+} \rightarrow ZnO + H_2O + 2OH^- \quad (4)$$

The synthesis mechanism underlying the formation of ZnO MFs composed of nanorod structure hinges upon the initial precipitation of $Zn(OH)_2^{2+}$ and $[Zn(OH)_4^{2-}]^{2+}$ within a solution medium. In the mixed solution of zinc acetate and sodium hydroxide, the concentration of OH^- ions escalates with the concurrent rise in pH. Notably, the complex $Zn(OH)_2^{2+}$ and $[Zn(OH)_4^{2-}]^{2+}$ are predominantly generated when the solution's pH is above 9, with $[Zn(OH)_4^{2-}]^{2+}$ serving as the fundamental growth unit for wurtzite ZnO. Given the higher solubility of $Zn(OH)_2$ compared to ZnO precipitates, a continuous generation of Zn^{2+} and OH^- ions from $Zn(OH)_2$ precipitates fosters the formation of the ZnO nucleic. Under hydrothermal conditions, the growth rate of ZnO planes follows the sequence [001] > [111] > [110] > [111] > [001] [27]. In this work, the nanorod structures exhibited wide tips and bases attributed to thermal modifications during the stirring process, thereby enhancing the surface area of the ZnO MFs.

(a) **(b)**

Fig. 3 *ZnO nanomaterial (a) As-synthesized in solution; and (b) Powder form*

The initial characterization step involves UV-Vis analysis to evaluate the spectral absorbance of ZnO. As depicted in Figure 4(a), a distinct peak absorbance is discerned within the wavelength range of 350 – 380 nm [34]. Specifically, the peak is centered at 359.5 nm, exhibiting an absorbance value of 0.58813 a.u. Al-Gaashani *et al.* observed the absorption peak of the nanoflower structure is about 370 nm, produced via a microwave-assisted method [35].

Subsequent to UV-Vis, XRD characterization is conducted to elucidate the structural properties of ZnO, as illustrated in Figure 4(b). The XRD pattern reveals a prominent peak corresponding to the (101) plane, observed at an angle of 36.252^0. This significant finding suggests that the synthesized ZnO predominantly exhibits growth alignment along the (101) direction. Moreover, analysis of the XRD data yields crucial information regarding the crystal size, with the maximum direction exhibiting a size of 21.768 nm. Additionally, minor peaks are discerned in the (100), (002), (102), and (110) planes, contributing to the overall structural characterization of ZnO, as detailed in Table 1. The absence of any additional distraction peaks discernible in the XRD pattern corroborates the successful synthesis of ZnO crystals characterized by high purities. The hexagonal structure of ZnO belongs to the C_{6V}^4 space group, featuring two formula units within its primitive cell, with all atoms occupying the 2b sites

endowed with C_{3V} symmetry. According to the group theory, single-crystalline ZnO manifests six distinct optical phonon modes situated at the center of the Brillouin zone, enumerated as follows:

$$\Gamma = A_1 + 2B_1 + E_1 + 2E_2 \quad (4)$$

Among the phonon modes exhibited by wurtzite hexagonal ZnO single crystalline materials, only A_1, E_1, and E_2 demonstrate Raman activity. Additionally, A_1 and E_1 are not only Raman active but also infrared (IR) active, each exhibiting longitudinal optical and transverse optical components. The nonpolar phonon modes characterized by E_2 symmetry present two frequencies: E_{2H} correlated with oxygen atoms and E_{2L} linked to the Zn sublattice [36]–[38].

Furthermore, FESEM is employed to elucidate the morphological properties of ZnO MFs, as depicted in Figure 4(c). The obtained image reveals the characteristic of the flower morphology of ZnO that consists of a nanorod structure with a fused base, with detailed measurements indicating an average length, width, and aspect ratio of 5.47 ± 0.84 µm, 1.30 ± 0.26 µm, and 4.35 ± 1.02, respectively. The adoption of a microflower structure is deliberate, as it offers a high surface-to-volume ratio, enhancing sensitivity to the target analyte [39], [40].

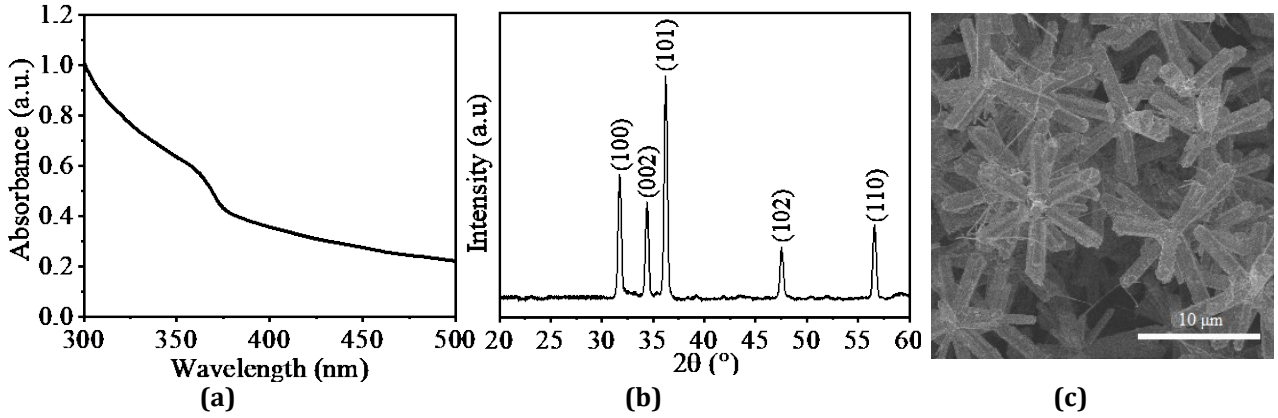

Fig. 4 *Characterization of ZnO MFs using (a) UV-Vis; (b) XRD; and (c) FESEM*

Table 1 *The detailed position of each plane for XRD*

Plane	2θ (◦)	Intensity (a.u)	FWHM	Crystal size (nm)
100	31.767	5348.92	0.3936	20.984
002	34.420	3897.77	0.3346	24.854
101	36.252	9221.71	0.3840	21.768
102	47.537	2151.45	0.2160	40.187
110	56.593	2975.85	0.3360	26.852

3.2 Optical Sensor Testing

The initial testing involves the optical sensor's capability to detect profenofos and diazinon through optical response testing, depicted in Figure 5. Analysis reveals that ZnO in the profenofos and diazinon mediums exhibit a diminished response compared to instances of pure ZnO and DIW medium. Notably, a negligible response is observed in the case of pure profenofos and diazinon without ZnO, indicating the pivotal role of ZnO in generating a distinctive spectral response influenced by changes in the surrounding medium. Detailed information regarding the specific starting points of each sample is provided in Table 2, facilitating a comprehensive interpretation of the obtained results.

Int. Journal of Integrated Engineering Vol. 17 No. 1 (2025) p. 451-462

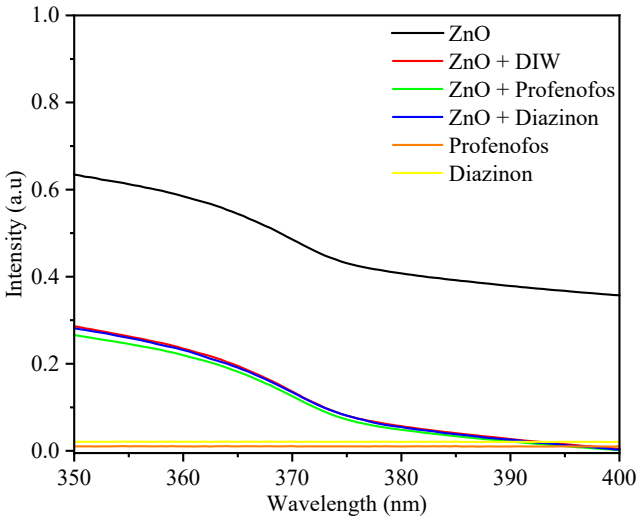

Fig. 5 *Optical responses in various mediums*

Table 2 *The detailed starting point for optical response testing in various mediums*

Medium	Starting Point (a.u)
Pure ZnO	0.634
ZnO + DIW	0.286
ZnO + Profenofos	0.266
ZnO + Diazinon	0.282
Pure Profenofos	0.010
Pure Diazinon	0.021

The profenofos are mixed with ZnO MFs as a sensing material and put in the transparent cuvette with a ratio of 1 : 5. Sensor testing is systematically conducted across a concentration range spanning from 1 to 10,000 ppm. The obtained sensor responses are presented in Figure 6(a), revealing discernible distinctions between profenofos and DIW as a reference. Moreover, notable variations in sensor responses are observed in correspondence with different profenofos concentrations, validating the functionality of the optical sensor. Specifically, the sensor exhibits the lowest starting point with profenofos concentration at 1 ppm, registering at 0.266 a.u. Conversely, the highest initial reading is recorded with profenofos concentration at 10,000 ppm, yielding a value of 0.285 a.u. This condition is influenced by the refractive index change of the targeted analyte, leading to stronger light-matter interactions and increasing the optical sensor response [41].

Following the acquisition of sensor responses, subsequent data processing involves calculating the Absolute Optical Change (AOC) value for profenofos testing. AOC is defined as the absolute difference between the analyte absorbance and reference absorbance [42], [43], as illustrated in Figure 6(b). Examination of the AOC values reveals that the highest magnitude is attained when profenofos concentration is at 1 ppm. This observation signifies that the optical sensor exhibits its maximum performance in detecting profenofos at this concentration threshold. The AOC value directly correlates with the sensor's ability to detect and quantify targeted analyte, with a higher value signifies a more sensitive sensor response to the analyte [44]–[46].

Next, the diazinon is mixed with ZnO MFs as a sensing material, and the ratio used is 1 : 5. The mixing is done to produce the optical phenomenon so that detection can be carried out. The sensor response of ZnO in DIW and various concentrations of diazinon is shown in Figure 6c. Based on Figure 6c, this test obtains a different response between diazinon and DIW. Furthermore, this test also received a different response when the optical sensor detected diazinon with different concentrations, proving that the built optical sensor functioned well in diazinon detection. Then, Figure 6d shows the AOC value for diazinon detection. Based on this figure, the maximum AOC value is obtained when the diazinon analyte has a concentration of 100 ppm. This result indicated that the optical sensor's maximum performance limit in detecting diazinon is 100 ppm.

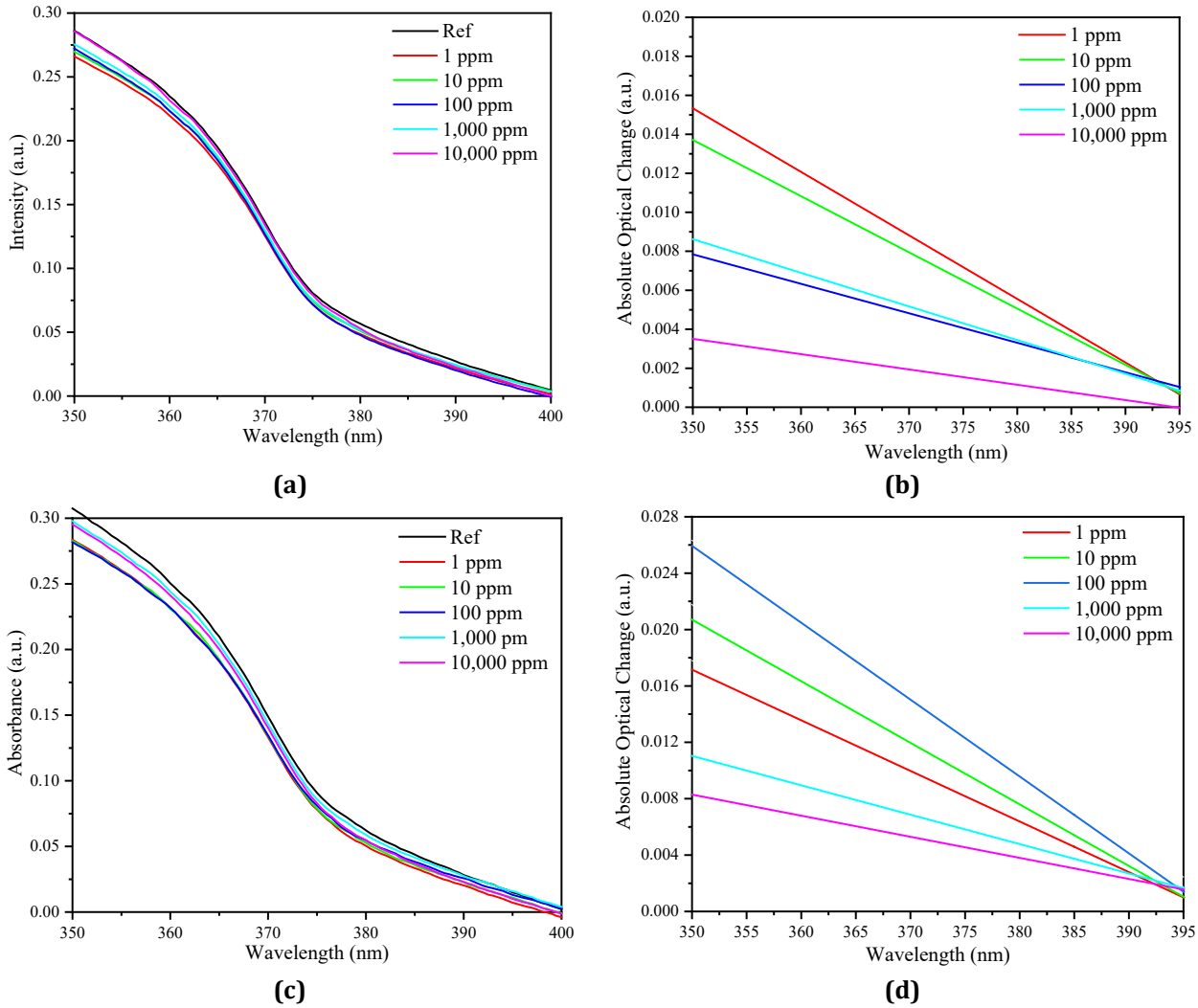

Fig. 6 *Sensor response towards (a -b) Profenofos; and (c -d) Diazinon. Optical response in various concentrations shown for (a) Profenofos; and (c) Diazinon. AOC value illustrates for (b) Profenofos; and (d) Diazinon*

The a-value derived from the linear regression equation $y = ax + b$, as depicted in Figure 6b for profenofos detection, serves as a crucial determinant in assessing the sensitivity of the optical sensor, encapsulating both the slope and the intersection point of the sensor response curve. The optical sensor's sensitivity in detecting profenofos is comprehensively documented in Table 3, accompanied by the sensitivity curve illustrated in Figure 7a. Analysis of Table 3 and Figure 7a reveals that optimal sensitivity is attained when the optical sensor detects profenofos at a concentration of 1 ppm. However, sensitivity diminishes as the sensor detects profenofos concentrations exceeding 1 ppm.

The a-value from the linear regression equation $y = ax + b$, obtained in Figure 6d for diazinon detection, is used to determine the sensitivity value of the optical sensor because it shows the slope and the intersection point of the sensor response. The optical sensor sensitivity in diazinon detection is shown in Table 3, with the sensitivity curve shown in Figure 7b. Based on this data, the highest sensitivity is obtained when detecting diazinon in the concentration of 100 ppm. Meanwhile, the sensitivity of the optical sensor will decrease in the concentration of 1,000 ppm and 10,000 ppm. The diazinon test result shows that this system's Limit of Detection (LoD) is 1 ppm.

Table 3 *Sensitivity of optical sensor towards profenofos and diazinon testing*

Concentration (ppm)	Sensitivity towards profenofos ($\times 10^{-5}$RIU)	Sensitivity towards diazinon ($\times 10^{-5}$ RIU)
1	33	36
10	19	44
100	15	55
1,000	17	21
10,000	8	15

Int. Journal of Integrated Engineering Vol. 17 No. 1 (2025) p. 451-462

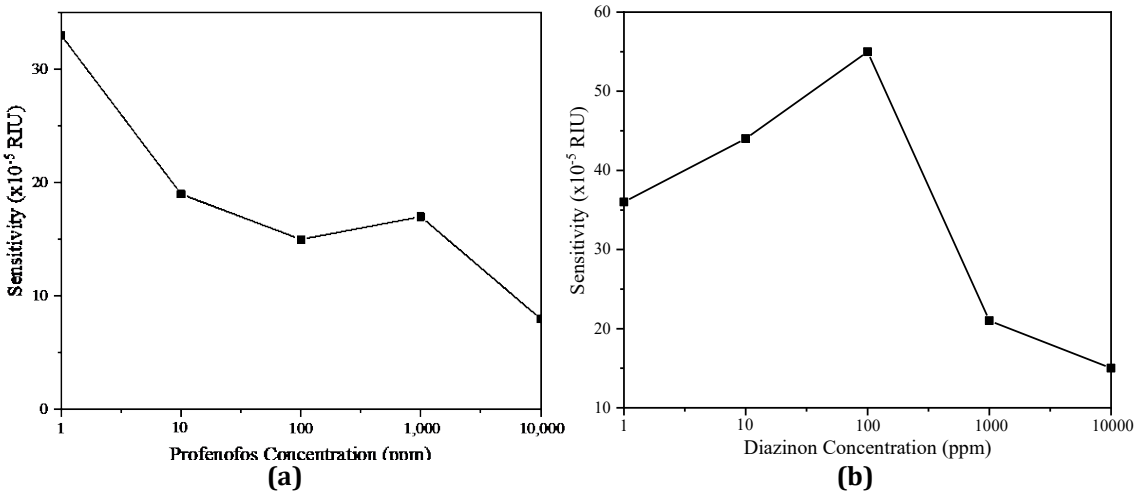

Fig. 7 *Sensitivity response of each (a) Profenofos; and (b) Diazinon concentration*

Table 4 compares the performance of the optical sensor with chromatography in detecting organophosphate pesticides [47]. They modified by equipping the system with a phosphorus flame photometric detector. Even though modifications have been made, the required detection time for diazinon is at least 1 hour. Based on this, it can be concluded that the optical sensor can be used as an alternative for detecting pesticides and can replace conventional methods such as chromatography because short detection time, is cheap, and is easy to use. The disadvantages of this system are its low sensitivity and high detection limit value, so the challenge in developing this system is increasing sensitivity and reducing the limit of detection to less than 1 ppm.

Table 4 *Comparison of several methods in detecting organophosphate pesticide*

Method	Detection time	LoD	Cost	Need of experts	Remark
Optical sensor (this work)	1 second	1 ppm	Cheap	No	Simple
Gas Chromatography [47]	> 1 hour	0.3764 ppm	Expensive	Yes	Complicated, analyte treatment
ELISA [13]	2 – 4 hours	0.2 ppm	Cheap	Yes	Complicated, requires specific antibody
Mass Spectrometry [15]	> 1 hour	-	Expensive	Yes	Complicated, analyte treatment
Electrochemical [16]	15 – 30 minutes	0.0001 ppm	Cheap	No	Simple
VIS/NIR spectroscopy [17]	-	0.01	Cheap	Yes	Moderate, needs calibration
HPLC [18]	> 30 minutes	0.1	Expensive	Yes	Complicated, needs optimization

4. Conclusion

An optical sensor for profenofos and diazinon detection has been successfully developed. Leveraging ZnO with a microflower morphology as the sensing material, given its inherently high surface area, renders it particularly sensitive to the targeted analyte, namely profenofos and diazinon. In the experimental phase, profenofos and diazinon concentrations ranging from 1 to 10,000 ppm are selected, yielding distinct optical spectra indicative of significant differences across varying concentrations. This compelling evidence underscores the optical sensor's efficacy in accurately detecting profenofos and diazinon. Moreover, the LoD for the system is established at 1 ppm, affirming its capability to discern minute profenofos and diazinon concentrations. Notably, employing the AOC value as a sensing parameter reveals optimal sensitivity at 1 ppm for profenofos and 100 ppm for diazinon, indicative of the system's peak response. Consequently, there exists a pertinent need for further development targeting organophosphate pesticide concentrations below 1 ppm to bolster comprehensive detection capabilities.

Acknowledgement

The author would like to thank Direktorat Riset, Teknologi, dan Pengabdian kepada Masyarakat, Direktorat Jenderal Pendidikan Tinggi, Riset, dan Teknologi, Kementerian Pendidikan, Kebudayaan, Riset, dan Teknologi Republik Indonesia for providing research grant (Contract No. 1570af/IT9.2.1/PT.01.03/2024).

Conflict of Interest

The authors declare that there is no conflict of interest regarding the publication of the paper.

Author Contribution

The authors confirm their contribution to the paper as follows: ***Analysis and draft manuscript preparation:*** *Natasya Salsabiila;* ***study conception, analysis, and editor:*** *Suratun Nafisah & Lukman Nulhakim;* ***data collection and analysis:*** *Bambang Irawan Tanjung & Nur Liyana Razali;* ***study conception and supervision:*** *Marlia Morsin;* ***editor and proofread:*** *Muhammad Reza Kahar Aziz. All authors reviewed the results and approved the final version of the manuscript.*

References

[1] Rajagopalan, V., Venkataraman, S., Rajendran, D. S., Kumar, V. V., Kumar, V. V., & Rangasamy, G. (2023). Acetylcholinesterase biosensors for electrochemical detection of neurotoxic pesticides and acetylcholine neurotransmitter: A literature review. *Environmental Research*, 115724. https://doi.org/10.1016/j.envres.2023.115724

[2] Araújo, M. F., Castanheira, E. M. S., & Sousa, S. F. (2023). The buzz on insecticides: a review of uses, molecular structures, targets, adverse effects, and alternatives. *Molecules*, *28*(8), 3641. https://doi.org/10.3390/molecules28083641

[3] Kumaran, A., Vashishth, R., Singh, S., Surendran, U., James, A., & Chellam, P. V. (2022). Biosensors for detection of organophosphate pesticides: Current technologies and future directives. *Microchemical Journal*, 107420. https://doi.org/10.1016/j.microc.2022.107420

[4] Tudi, M., Li, H., Li, H., Wang, L., Lyu, J., Yang, L., Tong, S., Yu, Q. J., Ruan, H. D., & Atabila, A. (2022). Exposure routes and health risks associated with pesticide application. *Toxics*, *10*(6), 335. https://doi.org/10.3390/toxics10060335

[5] Perry, J., Cotton, J., Rahman, M. A., & Brumby, S. A. (2020). Organophosphate exposure and the chronic effects on farmers: a narrative review. *Rural and Remote Health*, *20*(1). https://doi.org/10.22605/RRH4508

[6] Vigneshwaran, S., Preethi, J., Park, C. M., & Meenakshi, S. (2021). In-situ fabrication of ternary (3D/2D/2D) prism–like structures with dramatically enhancement on degradation of profenofos: A systemic study. *Journal of Water Process Engineering*, *39*, 101720. https://doi.org/10.1016/j.jwpe.2020.101720

[7] Parmar, D., Vaghela, N., & Rank, J. (2022). *Profenofos degradation and plant growth promoting potential bacterial isolate S. Paucimobilisdn-5*. *4*(1), 26–36. https://doi.org/10.33545/26649926.2022.v4.i1a.38

[8] Nesakumar, N., Suresh, I., Jegadeesan, G. B., Rayappan, J. B. B., & Kulandaiswamy, A. J. (2022). An efficient electrochemical sensing platform for profenofos detection. *Measurement*, *202*, 111807. https://doi.org/10.1016/j.measurement.2022.111807

[9] Yigit, N., & Velioglu, Y. S. (2020). Effects of processing and storage on pesticide residues in foods. *Critical Reviews in Food Science and Nutrition*, *60*(21), 3622–3641. https://doi.org/10.1080/10408398.2019.1702501

[10] Ismail, B., & Nielsen, S. S. (2010). Basic principles of chromatography. *Food Analysis*, *27*, 473–498. https://doi.org/10.1007/978-1-4419-1478-1_27

[11] Wani, A. A., Dar, A. A., Jan, I., Mukhtar, M., Sofi, K. A., Hassan, G. I., & Sofi, J. A. (2022). Dissipation and gas chromatographic method for the determination of profenofos residues in/on green pea and cucumber. *Biomedical Chromatography*, *36*(4), e5335. https://doi.org/10.1002/bmc.5335

[12] Clark, B. R., & Engvall, E. (2018). Enzyme-linked immunosorbent assay (ELISA): Theoretical and practical aspects. In *Enzyme-immunoassay* (pp. 167–180). CRC Press.

[13] Wu, K.-H., Huang, W.-C., Chang, S.-C., & Shyu, R.-H. (2022). Colloidal silver-based lateral flow immunoassay for detection of profenofos pesticide residue in vegetables. *RSC Advances*, *12*(21), 13035–13044. https://doi.org/10.1039/D2RA01654K

[14] García-León, M. (2022). Principles of mass spectrometry. In *Detecting Environmental Radioactivity* (pp. 495–519). Springer. https://doi.org/10.1007/978-3-031-09970-0_16

[15] Angthararuk, D., Harir, M., Schmitt-Kopplin, P., Sutthivaiyakit, S., Kettrup, A., & Sutthivaiyakit, P. (2017). Degradation products of profenofos as identified by high-field FTICR mass spectrometry: Isotopic fine structure approach. *Journal of Environmental Science and Health, Part B*, *52*(1), 10–22. https://doi.org/10.1080/03601234.2016.1224696

[16] Zahirifar, F., Rahimnejad, M., Abdulkareem, R. A., & Najafpour, G. (2019). Determination of Diazinon in fruit samples using electrochemical sensor based on carbon nanotubes modified carbon paste electrode. *Biocatalysis and Agricultural Biotechnology*, *20*, 101245. https://doi.org/https://doi.org/10.1016/j.bcab.2019.101245

[17] Jamshidi, B., Mohajerani, E., Jamshidi, J., Minaei, S., & Sharifi, A. (2015). Non-destructive detection of pesticide residues in cucumber using visible/near-infrared spectroscopy. *Food Additives & Contaminants. Part A, Chemistry, Analysis, Control, Exposure & Risk Assessment*, *32*(6), 857–863. https://doi.org/10.1080/19440049.2015.1031192

[18] Mohammadzaheri, R., Dogaheh, M. A., Kazemipour, M., & Soltaninejad, K. (2019). Optimization and validation of a novel nebulizer-assisted liquid phase microextraction followed by hplc-dad for diazinon analysis in plasma samples. *International Journal of Medical Toxicology and Forensic Medicine*, *9*(4), 221–232. https://doi.org/10.32598/ijmtfm.v9i4.26167

[19] Peltomaa, R., Glahn-Martínez, B., Benito-Peña, E., & Moreno-Bondi, M. C. (2018). Optical biosensors for label-free detection of small molecules. *Sensors*, *18*(12), 4126. https://doi.org/10.3390/s18124126

[20] Park, J.-H., Cho, Y.-W., & Kim, T.-H. (2022). Recent advances in surface plasmon resonance sensors for sensitive optical detection of pathogens. *Biosensors*, *12*(3), 180. https://doi.org/10.3390/bios12030180

[21] Zhang, M., Kong, Q., Huang, J., Xiang, Y., Wang, G., Han, J., Guo, Y., Zhao, S., & Sun, X. (2022). Electrochemiluminescence aptasensor based on 3D flower-like ZnONPs catalysis for the detection of diazinon in vegetables. *Sensors and Actuators B: Chemical*, *361*, 131690. https://doi.org/10.1016/j.snb.2022.131690

[22] Verma, R., Pathak, S., Srivastava, A. K., Prawer, S., & Tomljenovic-Hanic, S. (2021). ZnO nanomaterials: Green synthesis, toxicity evaluation and new insights in biomedical applications. *Journal of Alloys and Compounds*, *876*, 160175. https://doi.org/10.1016/j.jallcom.2021.160175

[23] Zhang, H., Chen, W., Li, Y., Song, Z., Zeng, W., Tang, S., Wang, S., & Zhou, D. (2020). Hierarchical heterostructures of nanosheet-assembled NiO-modified ZnO microflowers for high performance acetylene detection. *Ceramics International*, *46*(3), 3574–3581. https://doi.org/10.1016/j.ceramint.2019.10.075

[24] Quan, Y., Yao, J., Yang, S., Chen, L., Li, J., Liu, Y., Lang, J., Shen, H., Wang, Y., & Wang, Y. (2019). ZnO nanoparticles on MoS2 microflowers for ultrasensitive SERS detection of bisphenol A. *Microchimica Acta*, *186*, 1–8. https://doi.org/10.1007/s00604-019-3702-4

[25] Umar, A., Ibrahim, A. A., Alhamami, M. A., Algadi, H., Ahmed, F., Hussain, S., Fouad, H., & Akbar, S. (2022). ZnO nanorods assembled microflower-based gas sensor for detecting formaldehyde. *Materials Express*, *12*(12), 1481–1487. https://doi.org/10.1166/mex.2022.2315

[26] Zhang, W., Song, L., Zhao, D., Liu, T., Jiang, H., Yang, W., Zhao, B., Huang, W., Wang, P., & Sui, L. (2023). Construction of hierarchical ZnO flower-like structure for boost H_2S detection at low temperature. *Sensors and Actuators B: Chemical*, *385*, 133728. https://doi.org/10.1016/j.snb.2023.133728

[27] Wahab, R., Kim, Y. S., Mishra, A., Yun, S. Il, & Shin, H. S. (2010). Formation of ZnO micro-flowers prepared via solution process and their antibacterial activity. *Nanoscale Research Letters*, *5*(10), 1675–1681. https://doi.org/10.1007/s11671-010-9694-y

[28] An'Nisa, N. Z., Morsin, M., Sanudin, R., Razali, N. L., & Nafisah, S. (2020). Controlled wet chemical synthesis of gold nanorods for triclopyr butotyl herbicide detection based-plasmonic sensor. *Sensing and Bio-Sensing Research*, *29*, 100359. https://doi.org/10.1016/j.sbsr.2020.100359

[29] Salsabiila, N., Morsin, M., Hasbullah, M. H., Nafisah, S., Razali, N. L., & Iwantono. (2024). Thiol functionalized gold nanobipyramids-based plasmonic sensor for glucose detection. *IIUM Engineering Journal*, *25*(1 SE-Materials and Manufacturing Engineering), 274–290. https://doi.org/10.31436/iiumej.v25i1.2811

[30] Salsabiila, N., Morsin, M., Nafisah, S., Razali, N. L., Mahmud, F., & Alip, A. A. (2024). Investigation of the effect of amine and thiol as functional groups on gold nanobipyramids properties. *Materialia*, 102072. https://doi.org/10.1016/j.mtla.2024.102072

[31] Nafisah, S., Morsin, M., Jumadi, N. A., Nayan, N., Mohd Shah, N. S., Razali, N. L., & An'nisa, N. Z. (2020). Improved sensitivity and selectivity of direct localized surface plasmon resonance sensor using gold nanobipyramids for glyphosate detection. *IEEE Sensors Journal*, *20*(5), 2378–2389. https://doi.org/10.1109/JSEN.2019.2953928

[32] Morsin, M., Salleh, M. M., Umar, A. A., & Sahdan, M. Z. (2017). Gold nanoplates for a localized surface plasmon resonance-based boric acid sensor. *Sensors (Switzerland)*, *17*(5), 1–9. https://doi.org/10.3390/s17050947

[33] Nengsih, S., Umar, A. A., Salleh, M. M., & Oyama, M. (2012). Detection of formaldehyde in water: A shape-effect on the plasmonic sensing properties of the gold nanoparticles. *Sensors*, *12*(8), 10309–10325. https://doi.org/10.3390/s120810309
[34] Chieng, B. W., & Loo, Y. Y. (2012). Synthesis of ZnO nanoparticles by modified polyol method. *Materials Letters*, *73*, 78–82. https://doi.org/10.1016/j.matlet.2012.01.004
[35] Al-Gaashani, R., Radiman, S., Daud, A. R., Tabet, N., & Al-Douri, Y. (2013). XPS and optical studies of different morphologies of ZnO nanostructures prepared by microwave methods. *Ceramics International*, *39*, 2283–2292. https://doi.org/10.1016/j.ceramint.2012.08.075
[36] Nowak, E., Szybowicz, M., Stachowiak, A., Koczorowski, W., Schulz, D., Paprocki, K., Fabisiak, K., & Los, S. (2020). A comprehensive study of structural and optical properties of ZnO bulk crystals and polycrystalline films grown by sol-gel method. *Applied Physics A*, *126*(7), 552. https://doi.org/10.1007/s00339-020-03711-2
[37] Khai, T. V, Long, L. N., Khoi, N. H., & Hoc Thang, N. (2022). Effects of hydrothermal reaction time on the structure and optical properties of ZnO/graphene oxide nanocomposites. In *Crystals* (Vol. 12, Issue 12). https://doi.org/10.3390/cryst12121825
[38] Huang, R., Zhang, S., Zhang, W., & Yang, X. (2021). Progress of zinc oxide-based nanocomposites in the textile industry. *IET Collaborative Intelligent Manufacturing*, *3*(3), 281–289. https://doi.org/10.1049/cim2.12029
[39] Jagadale, S. B., Patil, V. L., Vanalakar, S. A., Patil, P. S., & Deshmukh, H. P. (2018). Preparation, characterization of 1D ZnO nanorods and their gas sensing properties. *Ceramics International*, *44*(3), 3333–3340. https://doi.org/10.1016/j.ceramint.2017.11.116
[40] Rai, P., Kim, Y. S., Song, H. M., Song, M. K., & Yu, Y. T. (2012). The role of gold catalyst on the sensing behavior of ZnO nanorods for CO and NO2 gases. *Sensors and Actuators, B: Chemical*, *165*(1), 133–142. https://doi.org/10.1016/j.snb.2012.02.030
[41] Silva, V. M. da, Filho, J. F. M., & Nascimento, J. F. do. (2021). Cascaded refractive index and corrosion sensors in a D-Shaped optical fiber using LMR and SPR effects. *2021 SBFoton International Optics and Photonics Conference (SBFoton IOPC)*, 1–5. https://doi.org/10.1109/SBFotonIOPC50774.2021.9461953
[42] Della Gaspera, E., Guglielmi, M., Martucci, A., Giancaterini, L., & Cantalini, C. (2012). Enhanced optical and electrical gas sensing response of sol-gel based NiO-Au and ZnO-Au nanostructured thin films. *Sensors and Actuators, B: Chemical*, *164*(1), 54–63. https://doi.org/10.1016/j.snb.2012.01.062
[43] Tan, C. H., Tan, S. T., Lee, H. B., Ginting, R. T., Oleiwi, H. F., Yap, C. C., Jumali, M. H. H., & Yahaya, M. (2017). Automated room temperature optical absorbance CO sensor based on In-doped ZnO nanorod. *Sensors and Actuators, B: Chemical*, *248*, 140–152. https://doi.org/10.1016/j.snb.2017.02.161
[44] Bhat, P., & Naveen Kumar, S. K. (2022). Evaluation of IDE-based flexible thin film ZnO sensor for VOC sensing in a custom designed gas chamber at room temperature. *Journal of Materials Science: Materials in Electronics*, *33*(3), 1529–1541. https://doi.org/10.1007/s10854-021-07664-x
[45] Yuan, Z., Li, J., Zhang, R., & Meng, F. (2022). UV-light assisted high-performance n-propanol sensor based on rod-like co-modified ZnO at room temperature. *IEEE Sensors Journal*, *22*(14), 13882–13890. https://doi.org/10.1109/JSEN.2022.3182753
[46] Divedi, R. D., Bhattacharyya, T. K., & Sasmal, M. (2023). Solution process synthesis of MoS_2–BSA–ZnO nano–bio composite for ultralow-level Hg^2+ sensing applications. *IEEE Sensors Journal*, *23*(4), 3423–3430. https://doi.org/10.1109/JSEN.2023.3233981
[47] Aung, O., Soe, O. O., Sein, N. N., Nyaing, K., & Myint, A. (2020). Analysis of dimethoate and diazinon pesticide residues in soil by gas chromatography. *Myanmar Acad. Arts Sci. XVIII (1A)*, *XVIII*(1).